



Optics Letters

Erbium-doped lithium niobate waveguide amplifier enhanced by an inverse-designed on-chip reflector

ZHIWEI WEI,¹ JIANGWEI WU,¹ CHENGYU CHEN,¹ HAO LI,¹ WENJIE WAN,^{1,2} 
XIANFENG CHEN,^{1,3} AND YUPING CHEN^{1,*} 

¹State Key Laboratory of Photonics and Communications, School of Physics and Astronomy, Shanghai Jiao Tong University, Shanghai 200240, China

²University of Michigan-Shanghai Jiao Tong University Joint Institute, Shanghai Jiao Tong University, Shanghai, China

³Collaborative Innovation Center of Light Manipulations and Applications, Shandong Normal University, Jinan 250358, China

*ypchen@sjtu.edu.cn

Received 11 March 2025; revised 1 May 2025; accepted 1 May 2025; posted 2 May 2025; published 23 May 2025

This study presents a 3.6-cm-long erbium-doped lithium niobate waveguide amplifier enhanced by an inverse-designed on-chip reflector. Integrating a reflector to reflect signal light (1531.6 nm) at the waveguide end yielded an internal net gain of 40.5 dB, achieving a 17.3 dB gain improvement compared to a comparable reflector-free amplifier under small signal conditions. These results highlight a novel strategy, to the best of our knowledge, for optimizing integrated optical amplifiers, combining high gain with simplified architecture. The approach holds promise for advancing high-density photonic integrated systems, demonstrating the efficacy of inverse design in tailoring photonic device performance for practical applications. © 2025 Optica Publishing Group. All rights, including for text and data mining (TDM), Artificial Intelligence (AI) training, and similar technologies, are reserved.

<https://doi.org/10.1364/OL.561831>

As the cornerstone of modern telecommunications infrastructure, the erbium-doped fiber amplifier (EDFA) has been essential for high-capacity, long-haul data transmission since its invention in the late 1980s [1]. The unique optical properties of erbium ions, particularly their stable transitions and long excited-state lifetime, enable broad gain spectra across the conventional telecommunications C-band. This makes EDFAs particularly well-suited for amplifying multiple wavelengths at high bit rates. The success of erbium-doped fibers has driven efforts to integrate erbium ions into other waveguide platforms, leading to the development of erbium-doped waveguide amplifiers (EDWAs) [2]. Over the years, various host materials and waveguide designs have been explored, including ion-exchanged glass and lithium niobate waveguides, as well as planar waveguides in materials such as Al_2O_3 , Si_3N_4 , and Ta_2O_5 [3–7]. Among these materials, thin-film lithium niobate (TFLN) has become a preferred material in integrated optics due to its exceptional optical characteristics, including a high refractive index, broad transparency range, and strong electro-optic, acoustic-optic, and nonlinear optical responses [8,9]. This versatile platform has enabled numerous applications, such as ultra-compact frequency combs [10,11], high-speed electro-optic modulators [12,13], efficient wavelength converters [14,15], advanced

sensors [16–18], optical phased arrays [19], and integrated lasers [20–23]. On-chip optical amplifiers are critical components in integrated photonic systems. However, pure TFLN inherently lacks optical gain properties due to its non-radiative crystal structure and absence of rare-earth ion energy transitions, making standalone amplification unfeasible. Recent breakthroughs in erbium-doped TFLN waveguide amplifiers have demonstrated their viability as gain media [24–34]. As the pump light propagates further along the waveguide amplifiers, the intensity of the pump light decreases due to losses, which reduces the amplification effect of the signal light. Bidirectional pumping can improve this issue, resulting in a high pump intensity distribution at both ends and low in the middle. Compared to forward and backward pumping, bidirectional pumping has been demonstrated by researchers to provide the best amplification effect. Here, we present a new gain-enhancement strategy in an erbium-doped lithium niobate waveguide amplifier. An inverse-designed on-chip reflector was introduced into the end of the erbium-doped lithium niobate waveguide amplifier that can improve the internal net gain by about 17.3 dB compared to a comparable reflector-free amplifier.

The schematic illustration of the amplifier without a reflector and with a reflector is shown in Figs. 1(a) and 1(b). Longer amplifiers inherently carry higher risks of process-induced imperfections due to defect density scaling with the device length. The 3.6-cm-long amplifier was selected to balance chip footprint constraints and fabrication tolerance. Light from the fiber was coupled into a waveguide by an edge coupler and then went through an adiabatic waveguide taper until the width of the waveguide was $1.1\ \mu\text{m}$. It subsequently went through an adiabatic waveguide taper until the width of the waveguide was $9\ \mu\text{m}$. Single-mode optical field confinement was achieved by implementing a width-tapered waveguide structure. Reducing the waveguide width or the bend radius would increase optical losses due to enhanced sidewall scattering and radiative bending losses. In the bend region, we selected waveguides with a $2\ \mu\text{m}$ width and $200\ \mu\text{m}$ bend radius to balance propagation loss and amplifier footprint constraints. At the end of the amplifier, the reflector was introduced in the waveguide with a width of $1.1\ \mu\text{m}$. The simulated fundamental TE mode in $9\text{-}\mu\text{m}$ -wide and $1.1\text{-}\mu\text{m}$ -wide waveguide at $1460\ \text{nm}$ and $1531.6\ \text{nm}$ is shown in

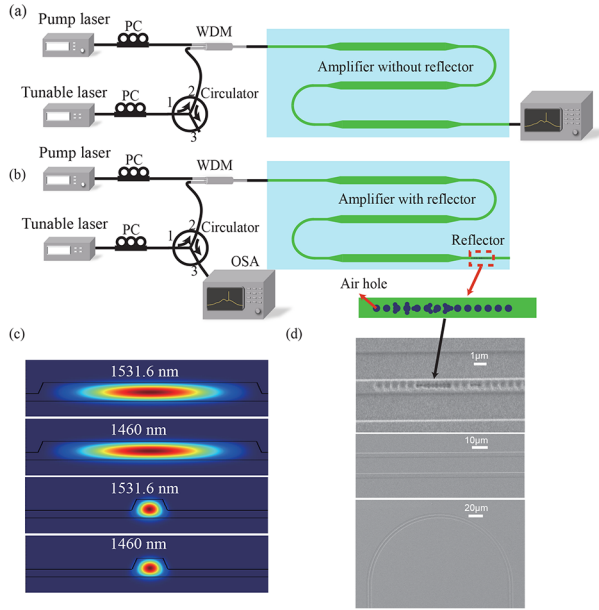


Fig. 1. Schematic illustration of the experimental setup. PC, polarization controller; WDM, wavelength division multiplexer; OSA, optical spectrum analyzer. (a) Schematic illustration of the experimental setup without a reflector. (b) Schematic illustration of the experimental setup with a reflector. (c) Simulated fundamental TE mode in 9- μm -wide and 1.1- μm -wide waveguide at 1460 nm and 1531.6 nm. (d) Scanning electron microscope (SEM) image of the waveguide and reflector.

Fig. 1(c). The thickness of TFLN is 600 nm. The etching depth of the erbium-doped TFLN waveguide is 350 nm. The angle of the sidewall is about 60° . The loss of the edge coupler in our experiment was about -7.7 dB/facet with an off-chip input signal power of 8.6 mW. The spot size of the lensed fiber is 2.5 μm , but the thickness of the TFLN is 600 nm, and the input taper width is 5 μm . The mismatch between the spot size of the lensed fiber and the size of the edge coupler is the main reason for the high coupling loss. The coupling losses can be improved by optimizing the design of the edge coupler in the future. The scanning electron microscope (SEM) images of the waveguide and reflector are shown in Fig. 1(d). The device is fabricated on an erbium-doped thin film lithium niobate by standard electron-beam lithography and reactive ion etching. Details of the fabrication process can be found in our previous work [35].

The design of the reflector consisted of two steps. First, similar to a Bragg reflector, a reflector for 1531.6 nm was designed to achieve light reflection through periodic air holes. The reflectivity is optimal, while the period of the air hole is 792.1 nm, and the top radius of the air hole is 263 nm. Inverse design enables researchers to systematically determine the parameters of photonic devices based on predefined objectives [36–40]. The workflow of inverse design involves four key steps: firstly, define a device or model composed of elements with tunable parameters x ; secondly, establish an objective function $f(x)$; thirdly, employ algorithms to iteratively adjust x , aiming to optimize $f(x)$; and finally, obtain the optimized parameters that best satisfy the objective.

In this work, inverse design was used to improve the reflector's reflectivity by introducing air holes with random positions and different sizes. The objective function was formulated as

$f(x) = R$. R is the reflectivity of the signal light with a wavelength of 1531.6 nm. The unit of the inverse design was an air hole. The sidewall of the lithium niobate waveguide has an angle. Both excessively large and small air hole radii in the unit cell led to suboptimal performance. Therefore, an intermediate radius (222 nm) was selected. The algorithm used in the inverse design was a genetic algorithm, which is similar to our previous work [41]. Due to the inclined sidewalls created during the etching process of thin-film lithium niobate, air holes with tapered profiles in the waveguide induce unintended optical leakage into the surrounding medium. By employing inverse design methods, irregularly shaped air holes can be strategically introduced to manipulate the optical propagation path. This approach can reduce both leakage losses and direct transmission, thereby enhancing the overall reflectivity of the waveguide structure. Considering a compact 10- μm -long reflector, a comparison of the reflectivity between the reflector with inverse design and the reflector without inverse design was shown in Fig. 2(a). The black line shows the result with inverse design, and the red line shows the result without inverse design. The performance of reflectors with inverse design in the range of 1520 nm–1540 nm is better than that of reflectors without inverse design. At 1531.6 nm, the reflectivity of the reflector with inverse design is 0.49, and the reflectivity of the reflector without inverse design is 0.43. The inverse design improved the reflectivity by 14%. The relation between the reactivity and fabrication error is shown in Fig. 2(b), showing an excellent fabrication tolerance.

Here, a quasi-two-level model [42] was used in our simulation. Ignoring the effects of spontaneous emission and excited-state absorption, the rate equations can be written as follows:

$$\frac{dN_1}{dt} = -(R_{12} + W_{12})N_1 + (A_{21} + R_{21} + W_{21})N_2, \quad (1)$$

$$\frac{dN_2}{dt} = -\frac{dN_1}{dt}, \quad (2)$$

$$N_0 = N_1 + N_2. \quad (3)$$

N_1 is the population density of energy level 1 ($^4I_{15/2}$), and N_2 is the population density of energy level 2 ($^4I_{13/2}$). N_0 is the total erbium-dopant concentration. The doping concentration of erbium-doped lithium niobate is 1 mol%, which corresponds to an Er^{3+} ion concentration of $1.9 \times 10^{20} \text{ cm}^{-3}$. The absorption and emission rates for the pump (signal) are denoted as R_{12} , W_{12} and R_{21} , W_{21} , respectively. The spontaneous transitions from the excited state to the ground state are represented by the rate $A_{21} = \frac{1}{\tau}$, where τ is the fluorescence lifetime.

In the case of steady state, the pump evolution and signal evolution along the propagation direction can be written as follows:

$$\frac{di_p}{dz} = [-\alpha_p + \sigma_{p,21}N_2 - \sigma_{p,12}N_1]i_p, \quad (4)$$

$$\frac{di_s}{dz} = [-\alpha_s + \sigma_{s,21}N_2 - \sigma_{s,12}N_1]i_s. \quad (5)$$

i_p is the intensity of the pump light and i_s is the intensity of the signal light. α_p is the propagation loss of the pump light, and α_s is the propagation loss of the signal light. $\sigma_{p,21}$ is the absorption cross section of the pump light, and $\sigma_{p,12}$ is the emission cross section of the pump light. $\sigma_{s,21}$ is the absorption cross section of the signal light, and $\sigma_{s,12}$ is the emission cross section of the signal light.

Considering a 3.6-cm-long waveguide, the pump evolution along the propagation direction is shown in Fig. 2(c). As the

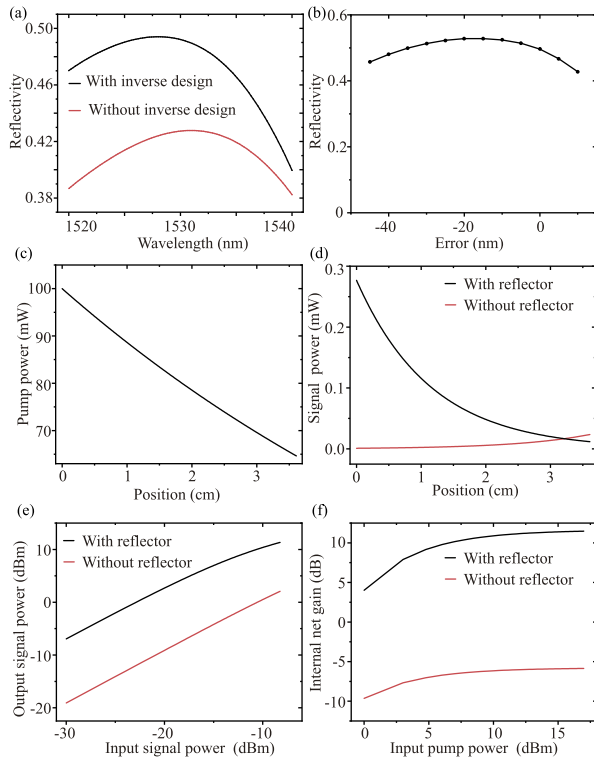


Fig. 2. Simulation result. (a) Comparison of the reflectivity between the reflector with inverse design (black) and the reflector without inverse design (red). (b) Relation between the reflectivity and fabrication error. (c) Relation between the on-chip pump power and position of the waveguide. (d) Relation between the signal power and position of the waveguide. (e) Relation between the output signal power and input signal power. (f) Relation between the gain and the input pump power.

propagation distance increases, the pump power decreases. After being amplified through forward propagation, the signal light is reflected by introducing a reflector at the end of the amplifier. After reflection, the intensity of the pump light gradually increases during the propagation of the signal light. In this way, the amplification effect of the signal light can be significantly enhanced. Considering the input signal light power as $1 \mu\text{W}$ and the pump power as 100 mW , the signal power at different positions is shown in Fig. 2(d). The black line shows the result with a reflector, and the red line shows the result without a reflector. Considering the pump power to be 100 mW , the relation between the output signal light power and the input signal power is shown in Fig. 2(e). During the small signal conditions, the amplification effect with a reflector is more than 13 dB higher than without a reflector. Considering the signal power to be $1 \mu\text{W}$, the relation between the gain and the input pump power is shown in Fig. 2(f).

The schematic illustration of the experimental setup is shown in Fig. 1. The signal light propagates through polarization controllers (PC) and a circulator. The pump light propagates through polarization controllers (PC). Both optical paths are then multiplexed by a wavelength division multiplexer (WDM) and coupled to the erbium-doped TFLN chip via a lensed fiber. In the amplifier with a reflector, the amplified signal light was first collected by the same lensed fiber with a spot size of $2.5 \mu\text{m}$, subsequently propagated through the WDM and circulator, and finally detected by the OSA. In the amplifier without

a reflector, the amplified signal light was collected by another lensed fiber and detected by the OSA. The signal light is generated by an external-cavity tunable laser operating in the telecom band (New Focus, $1520\text{--}1570 \text{ nm}$), with its power regulated using an optical attenuator. Conventional erbium-doped amplifiers typically utilize 980 nm or 1480 nm laser bands as pump sources. To optimize coupling efficiency between the pump and signal light through a shared lensed fiber, we selected the 1480 nm laser bands as pump sources due to its spectral proximity to the signal wavelength. However, constrained by the available source, a 1460 nm pump laser was experimentally adopted. The polarization states of both the signal and pump light are set to the TE_{00} mode using PC to ensure minimal loss and maximum net gain.

The amplified spontaneous emission (ASE) spectrum of the EDWA is shown in Fig. 3(a). The strongest spontaneous emission marked by the green dashed line occurs at 1531.6 nm . Selecting this wavelength as the wavelength of the signal light ensures maximum amplification efficiency, thereby optimizing the amplifier performance. The calculated propagation loss at 1531.6 nm is -1.44 dB/cm , using the measured Fabry–Perot fringes [43] as shown in Fig. 3(b). The performance characterization of the amplifier is shown in Fig. 4. The comparison of the output signal power between the amplifier with a reflector and the amplifier without a reflector is shown in Fig. 4(a). With an on-chip input pump power of 16.7 dBm and an on-chip input signal power of -42.9 dBm , the on-chip output signal power with a reflector is -12.8 dBm , while the on-chip output signal power without a reflector is -23.9 dBm . Under small signal amplification conditions, the output signal power of the amplifier with a reflector is 11.1 dB (12.9 times) greater than that of the amplifier without a reflector. The internal net gain can be used to characterize the amplifier’s performance, which can be formulated as follows: $G = 10 \log_{10} \frac{P_{out}}{P_{in}} - \alpha L$. G is the internal net gain. P_{out} is the output signal power, and P_{in} is the input signal power. α is the propagation loss including the scattering loss and the absorption loss [29]. L is the propagation distance. In the calculation of the internal net gain, the propagation loss is approximated to be -1.44 dB/cm . The relationship between the on-chip internal net gain and input signal power is shown in Fig. 4(b). The black line shows the result with a reflector, and the red line shows the result without a reflector. As the input signal power increases, the internal net gain decreases. The amplification performance of the amplifier with a reflector is significantly higher than that of the amplifier without a reflector. Under small signal conditions, with a fixed pump power of 16.7 dBm , the internal net gain of the amplifier with a reflector can reach 40.5 dB , while the internal net gain without a reflector is 23.2 dB . Compared to the amplifier without a reflector, the internal net gain of the amplifier with a reflector is improved by 17.3 dB (a 53.7 -fold increase). With an on-chip input signal power of -23.8 dBm , the relation of the on-chip pump power and the on-chip internal net gain is shown in Fig. 4(c). The simulation assumed fixed losses, whereas the absorption loss of erbium ions is power-dependent. Additionally, fabrication tolerances may exist. These factors collectively account for the discrepancies between the simulation and experimental results. Under varying pump power conditions, the amplification effect of the signal light in the amplifier with a reflector remains significantly higher than that in the amplifier without a reflector. The relationship between the on-chip internal net gain and wavelength is shown in Fig. 4(d). The results are consistent with the ASE spectrum.

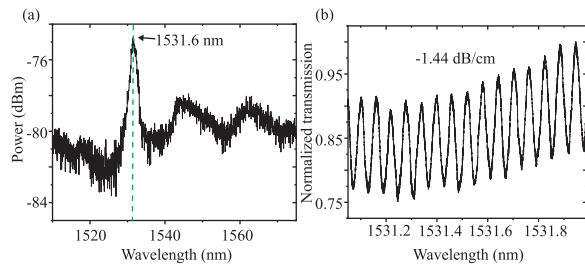


Fig. 3. (a) Amplified spontaneous emission (ASE) spectrum. (b) Measured Fabry–Perot fringes by the oscilloscope.

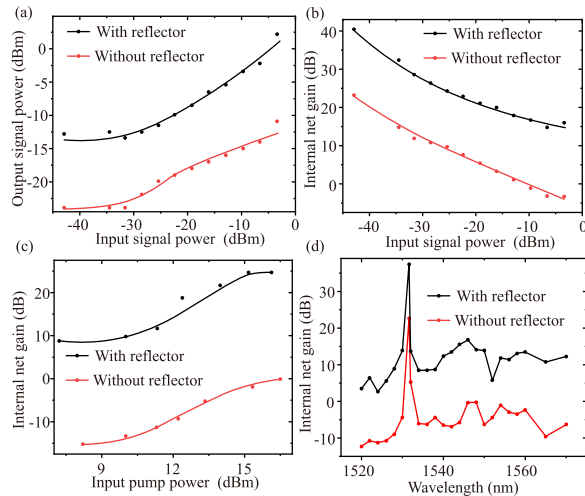


Fig. 4. (a) Relationship between the output signal power and input power. (b) Relationship between the on-chip internal net gain and input signal power. (c) Relationship between the on-chip internal net gain and pump power. (d) Relationship between the on-chip internal net gain and wavelength.

In conclusion, this research successfully realized an erbium-doped lithium niobate waveguide amplifier using inverse design. The on-chip reflector dramatically improved signal amplification (achieving 40.5 dB internal net gain). Experimental results demonstrated that the amplifier incorporating an inverse-designed reflector achieved a 17.3 dB (a 53.7-fold increase) improvement in internal net gain and a 12.9-fold increase in output signal power compared to its counterpart without the reflector. Combining simulations and experiments, this work highlights the potential of inverse-designed structures in optimizing photonic devices, offering a valuable reference for developing high-gain, low-complexity integrated amplifiers. These advancements could accelerate progress in optical communications and on-chip photonic systems.

Funding. National Natural Science Foundation of China (12134009, 12474335).

Acknowledgment. We acknowledge the Center for Advanced Electronic Materials and Devices (AEMD) of Shanghai Jiao Tong University for the fabrication support.

Disclosures. The authors declare no conflicts of interest.

Data availability. Data underlying the results presented in this paper are not publicly available at this time but may be obtained from the authors upon reasonable request.

REFERENCES

- P. M. Becker, A. A. Olsson, and J. R. Simpson, *Erbium-Doped Fiber Amplifiers: Fundamentals and Technology* (Elsevier, 1999).
- J. D. Bradley and M. Pollnau, *Laser Photonics Rev.* **5**, 368 (2011).
- G. Della Valle, S. Taccheo, P. Laporta, *et al.*, *Electron. Lett.* **42**, 632 (2006).
- R. Brinkmann, I. Baumann, M. Dinand, *et al.*, *IEEE J. Quantum Electron.* **30**, 2356 (1994).
- G. Van den Hoven, R. Koper, A. Polman, *et al.*, *Appl. Phys. Lett.* **68**, 1886 (1996).
- Z. Zhang, R. Liu, W. Wang, *et al.*, *Opt. Lett.* **48**, 5799 (2023).
- Y. Liu, Z. Qiu, X. Ji, *et al.*, *Science* **376**, 1309 (2022).
- Y. Qi and Y. Li, *Nanophotonics* **9**, 1287 (2020).
- P. Liu, H. Wen, L. Ren, *et al.*, *Front. Optoelectron.* **16**, 18 (2023).
- C. Wang, M. Zhang, M. Yu, *et al.*, *Nat. Commun.* **10**, 978 (2019).
- Y. He, Q.-F. Yang, J. Ling, *et al.*, *Optica* **6**, 1138 (2019).
- C. Wang, M. Zhang, X. Chen, *et al.*, *Nature* **562**, 101 (2018).
- Y. Xue, R. Gan, K. Chen, *et al.*, *Optica* **9**, 1131 (2022).
- Z. Hao, L. Zhang, W. Mao, *et al.*, *Photonics Res.* **8**, 311 (2020).
- J. Lu, J. B. Surya, X. Liu, *et al.*, *Optica* **6**, 1455 (2019).
- X. Wang, J. Wu, C. Chen, *et al.*, *Appl. Phys. Lett.* **124**, 061108 (2024).
- X. Wang, T. Yuan, J. Wu, *et al.*, *Laser Photonics Rev.* **18**, 2300760 (2024).
- T. Yuan, X. Wang, J. Wu, *et al.*, *Laser Photonics Rev.* **18**, 2400457 (2024).
- J. Wu, Z. Liang, X. Wang, *et al.*, *Opt. Lett.* **49**, 5087 (2024).
- Y. Liu, X. Yan, J. Wu, *et al.*, *Sci. China Phys. Mech. Astron.* **64**, 234262 (2021).
- V. Snigirev, A. Riedhauser, G. Lihachev, *et al.*, *Nature* **615**, 411 (2023).
- J. Wu, X. Yan, X. Wang, *et al.*, *ACS Photonics* **11**, 2114 (2024).
- Q. Luo, C. Yang, R. Zhang, *et al.*, *Opt. Lett.* **46**, 3275 (2021).
- J. Zhou, Y. Liang, Z. Liu, *et al.*, *Laser Photonics Rev.* **15**, 2100030 (2021).
- Z. Chen, Q. Xu, K. Zhang, *et al.*, *Opt. Lett.* **46**, 1161 (2021).
- Q. Luo, C. Yang, Z. Hao, *et al.*, *Chin. Opt. Lett.* **19**, 060008 (2021).
- X. Yan, Y. Liu, J. Wu, *et al.*, "Integrated spiral waveguide amplifiers on erbium-doped thin-film lithium niobate," *arXiv* (2021).
- M. Cai, K. Wu, J. Xiang, *et al.*, *IEEE J. Sel. Top. Quantum Electron.* **28**, 8200608 (2022).
- Y. Liang, J. Zhou, Z. Liu, *et al.*, *Nanophotonics* **11**, 1033 (2022).
- R. Bao, L. Song, J. Chen, *et al.*, *Opt. Lett.* **48**, 6348 (2023).
- R. Bao, Z. Fang, J. Liu, *et al.*, *Laser Photonics Rev.* **19**, 2400765 (2025).
- X. Xue, J. Qiu, T. Ding, *et al.*, *Opt. Mater. Express* **14**, 1985 (2024).
- Y. Chen, *Sci. China Phys. Mech. Astron.* **65**, 294231 (2022).
- Y. Jia, J. Wu, X. Sun, *et al.*, *Laser Photonics Rev.* **16**, 2200059 (2022).
- T. Yuan, J. Wu, Y. Liu, *et al.*, *Sci. China Phys. Mech. Astron.* **66**, 284211 (2023).
- X. He, D. Sun, J. Chen, *et al.*, *IEEE Photonics J.* **16**, 6600305 (2024).
- J. Lyu, T. Zhu, Y. Zhou, *et al.*, *Opto-Electronic Science* **2**, 230038 (2023).
- R. Shen, B. Hong, X. Ren, *et al.*, *J. Nanophoton.* **18**, 010901 (2024).
- C. Shang, J. Yang, A. M. Hammond, *et al.*, *ACS Photonics* **10**, 1019 (2023).
- S. Molesky, Z. Lin, A. Y. Piggott, *et al.*, *Nat. Photonics* **12**, 659 (2018).
- Z. Wei, J. Wu, C. Chen, *et al.*, *J. Opt. Soc. Am. B* **42**, 597 (2025).
- M. Dinand and W. Sohler, *IEEE J. Quantum Electron.* **30**, 1267 (1994).
- R. Regener and W. Sohler, *Appl. Phys. B* **36**, 143 (1985).